A Class of CFAR Detectors Implemented in the SAR-GMTI Processor *gmtipro2*

Mathematical Formulation of the Algorithms

M. Dragošević
MD TerraBytes Inc. (under subcontract to MDA Systems Ltd.)

W. Burwash
MDA Systems Ltd.

Prepared by:

MDA Systems Ltd.
75 Albert Street, Suite 412
Ottawa, ON K1P 5E7

Project Manager: G. Peake
Contract Number: W7714-081104/001/SV
Contract Scientific Authority: S. Chiu

Defence Research and Development Canada
Contract Report
DRDC Ottawa CR 2013-089
February 2015

Abstract

This document provides a detailed mathematical description of several detection algorithms that have been implemented in the Surface Moving Target Indicator (SMTI) processor *gmtipro2* and tested on the actual Synthetic Aperture Radar (SAR) data from RADARSAT-2 acquired in the Moving Object Detection Experiment (MODEX) mode. The common feature of the described algorithms is their Constant False Alarm Rate (CFAR) property. All of the detectors are generalized with respect to the number of available channels. Thus, they are defined both for Moving Object Detection Experiment 1 (MODEX1) and Moving Object Detection Experiment 2 (MODEX2) modes, which have two physical and four virtual channels, respectively. All of the detectors work in the image domain, but can be combined with Doppler Centroid (DC) offset focusing in order to integrate all signal energy and to improve the probability of detection. DC estimation, as one of the most important auxiliary algorithms, is also presented in the form of mathematical equations. The emphasis of the report is entirely on the mathematical formalism behind the computer code that implements these algorithms. Open literature references are provided regarding the derivation and analysis of these algorithms.

Résumé

Le document décrit de façon détaillée les équations qui sous-tendent plusieurs algorithmes de détection mis en œuvre dans le processeur *gmtipro2* indicateur de cibles terrestres mobiles (ICTM) et mis à l'essai à l'aide des données réelles du radar à synthèse d'ouverture (SAR) de RADARSAT-2 acquises en mode MODEX (Essais de détection d'objets en mouvement). Ces algorithmes partagent une caractéristique : leur taux de fausse alarme constant (TFAC). Tous les détecteurs peuvent traiter sont généralisés à l'ensemble des canaux disponibles ; ils peuvent donc traiter les données des modes MODEX1 (deux canaux physiques) et MODEX2 (quatre canaux virtuels). Tous les détecteurs travaillent à partir des représentations en images ; cependant, on peut les combiner à la focalisation du décalage du centroïde Doppler (DC) afin d'intégrer toute l'énergie des signaux et ainsi améliorer les chances de détecter toute cible mobile. Comme l'estimation du DC est l'un des algorithmes auxiliaires les plus importants, il est aussi présenté sous forme d'équations. Le rapport est entièrement consacré au formalisme mathématique qui sous-tend le code informatique mettant en œuvre ces algorithmes. Des documents de source ouverte sont cités sur la dérivation et l'analyse de ces algorithmes.

This page intentionally left blank.

Executive summary

A Class of CFAR Detectors Implemented in the SAR-GMTI Processor *gmtipro2* : Mathematical Formulation of the Algorithms

M. Dragošević, W. Burwash; DRDC Ottawa CR 2013-089; Defence Research and Development Canada; February 2015.

Background: A modular software architecture was developed at Defence Research and Development Canada (DRDC) to serve as a robust and efficient framework for a variety of signal processing algorithms. The intended purpose of this software, known as *gmtipro2*, is both operational and research oriented. Besides many general-purpose signal processing techniques, this architecture supports a number of detection and estimation methods that were developed specifically for the RADARSAT-2 Moving Object Detection Experiment (MODEX) data. The implementation of the detection and estimation algorithms started from the most basic ones and progressed towards more advanced approaches. For research purposes, it is highly desirable to provide a precise mathematical description of the implemented detection and estimation algorithms.

Principal results: A number of detection algorithms are presented in a unified and consistent way in full mathematical detail. The key equations are provided in a systematic way without the burden of implementation technicalities.

Significance of results: Detectors considered in this report come from a development line that was not previously specified. All of the presented algorithms are the result of incremental upgrades by the authors of the *gmtipro2* software. As such, this development line needed to be well documented. This presentation clarifies the main underlying concepts including parametric and non-parametric detection, reduced rank (projection) and full rank processing, selection of detection thresholds, Doppler offset processing and Doppler estimation. Mathematical expressions presented herein complement the other documentation on *gmtipro2*.

Future work: A comparison of different algorithms will follow as a separate study. It will compare the algorithms within and beyond the presented class using simulated and real-world moving targets.

Sommaire

A Class of CFAR Detectors Implemented in the SAR-GMTI Processor *gmtipro2* : Mathematical Formulation of the Algorithms

M. Dragošević, W. Burwash ; DRDC Ottawa CR 2013-089 ; Recherche et développement pour la défense Canada ; février 2015.

Contexte : Recherche et développement pour la défense Canada (RDDC) a développé une architecture logicielle modulaire afin de créer un cadre d'utilisation robuste et efficient de divers algorithmes de traitement des signaux. Ce logiciel, nommé *gmtipro2*, vise à servir tant à des fins opérationnelles qu'à la recherche. En plus de nombreuses techniques générales de traitement des signaux, cette architecture prend en charge des méthodes de détection et d'estimation propres aux données MODEX de RADARSAT-2. Pour mettre en œuvre les algorithmes de détection et d'estimation, on a commencé par les plus simples, puis on a graduellement mis en œuvre des algorithmes de plus en plus complexes. Il est impératif, aux fins de recherche, de décrire fidèlement les équations mathématiques utilisées dans la mise en œuvre des algorithmes de détection et d'estimation.

Principaux résultats : Divers algorithmes de détection sont présentés de façon uniforme et unifiée et expliqués en détail sous forme mathématique. Les équations les plus importantes sont systématiquement énoncées sans se soucier des détails de mise en œuvre.

Portée des résultats : Les algorithmes de détection traités dans le rapport découlent d'efforts de développement n'ayant pas été décrits auparavant. Comme tous les algorithmes présentés sont le fruit d'améliorations graduelles par les créateurs du logiciel *gmtipro2*, il est nécessaire de bien décrire les résultats de ces efforts. Le rapport décrit clairement les principaux concepts utilisés, notamment la détection paramétrique et non paramétrique, le traitement de rang réduit (projection) et de plein rang, le choix des seuils de détection ainsi que le traitement du décalage Doppler et l'estimation Doppler. Les expressions mathématiques présentées sont un complément à la documentation de *gmtipro2*.

Recherches futures : Une étude distincte comparera les divers algorithmes présentés dans le rapport et d'autres algorithmes à l'aide de cibles mobiles réelles et simulées.

Table of contents

List of figures

Acknowledgements

We thank: Dr. Shen Chiu and Dr. Chuck Livingstone for their constant support in developing, implementing and validating the algorithms documented in this report.

1 Background, Motivation and Objective

Defence Research and Development Canada (DRDC) has developed a powerful and versatile Synthetic Aperture Radar (SAR) Surface Moving Target Indicator (SMTI) processor known as *gmtipro2*. The software architecture of the *gmtipro2* processor allows the user to build a variety of algorithms using as building blocks the independently developed components, modules and plug-ins. An algorithm is implemented as a streamline of modules with their dependent pre-module and post-module plug-ins, as specified by the meta-data / configuration eXtensible Markup Language (XML) file. The processor can be used for innovative, research oriented, as well as standard processing, defined by several standard XML files.

Efficient usage of the processor depends on good understanding of its currently available components. It has been noted that many researchers prefer a rigorous mathematical formulation of the implemented algorithms to any other description, such as block diagrams, flow charts, pseudo-code or verbal. This is especially true for certain types of algorithms such as those described in this document.

The class of detectors considered in this report is not new. Their basic concept, rooted in the Likelihood Ratio Test (LRT), Maximum Likelihood (ML) and Generalized Likelihood Ratio Test (GLRT) approach, is well known and well published. However, there are many possible variations, specific details and enhancements, which actually make the difference. The objective of this document is to describe the implemented algorithms more precisely using mathematical formalisms and to provide a reliable single-source reference for these algorithms.

The set of equations presented herein describe the implemented algorithms very closely as their mathematical equivalents. They do not capture the organization, parallel execution, synchronization, interfaces, storage requirements, error handling or any other technical issue related to the *gmtipro2* design. Moreover, they are not necessarily transcribed into the C language corresponding to a single module or plug-in code. Only the mathematical concepts are captured.

2 Notation and Key System Parameters

This section summarizes the notation that is used throughout.

2.1 Common Symbols

By convention, bold lower case symbols are used for vectors and bold upper case symbols are used for matrices.

The following notation is used for common operations and mathematical units:

$(\cdot)^*$	Complex conjugate
$(\cdot)^T$	Transpose of a vector or matrix
$(\cdot)^H$	Hermitian transpose (transpose and complex conjugate)
$[\cdot]_n$	n-th component of a vector
$\langle\cdot\rangle$	Averaging
$\langle\cdot\rangle_x$	Averaging over argument x
j	Imaginary unit
$\mathbf{I}$	Unit (identity) matrix

The following symbols are used for some of the most common system parameters:

P	Number of Moving Object Detection Experiment (MODEX) channels (2 or 4)
λ	Radar wavelength
f_p	Pulse Repetition Frequency (PRF)
$D(\cdot)$	Baseline

The following symbols are used for some of the most important data-set parameters:

f_c	Doppler Centroid (DC)
V_s	Satellite speed in the Earth-Centered, Earth-Fixed (ECEF) referent system
V_r	Radial speed of the target

Signal and image coordinates are generally represented by the following symbols:

ζ	Slow time
τ	Fast time
x	Cross-range, along-track, azimuth index
y	Slant range, down range index

Signal and image processing makes use of the following standard symbols:

$s(\cdot)$	Signal sample
$\mathbf{s}(\cdot)$	Signal vector
$m(\cdot)$	Mask sample
σ^2	Variance of the signal or a signal component
$\mathbf{C}$	Covariance matrix
$\mathbf{P}^{\perp}$	Projection matrix
$\mathbf{b}(\cdot)$	Steering vector

More details regarding notation are provided in the following subsections.

2.2 Data Samples

It is convenient to represent the samples from P channels by a vector in the P-dimensional complex space $\mathbb{C}^P$, for example:

$$\mathbf{s}(x,y) = \begin{bmatrix} s(0,x,y) \\ \vdots \\ s(P-1,x,y) \end{bmatrix} \in \mathbb{C}^P \tag{1}$$

$$[\mathbf{s}(x,y)]_p = s(p,x,y) \tag{2}$$

where $p \in 0,\ldots,P-1$ is the channel index, x is the azimuth coordinate and y is the slant range coordinate. In words, the p-th component of the vector $\mathbf{s}(x,y)$ is the sample $s(p,x,y)$ from channel p. The same symbols, $s(\cdot)$ and $\mathbf{s}(\cdot)$, will be used in different algorithms to indicate the samples to which the algorithm is applied (original samples), which may be at any state of processing. Where the processing state (or a processing parameter) of the original samples matters, it will be verbally stated, as well as by additional symbols.

2.3 Data Masking

Many of the implemented algorithms accept data masking, which is used to indicate invalid or undesired data at some stage of processing. Examples include invalid image portions (wedges) after SAR focusing, land or water surfaces within algorithms specialized for a certain type of clutter, pixels outside a region of interest, pixels occupied by targets when background statistics are being estimated and so on. The symbol $m(x,y)$ will be used for the mask of any nature to indicate:

$$m(x,y) = \begin{cases} 1 & \text{for valid samples} \\ 0 & \text{for invalid samples} \end{cases} \tag{3}$$

Data masking is implemented simply as multiplication $m(x,y)\mathbf{s}(x,y)$ to discriminate between valid and invalid or undesired samples.

2.4 Averaging

Data averaging will symbolically be represented by $\langle\cdot\rangle$ and, as a rule, will include masking (with default masking $m(x,y) = 1$ for for all range and azimuth bins). For example

$$\langle \mathbf{s}(x,y)\rangle = \frac{\sum_x \sum_y m(x,y)\mathbf{s}(x,y)}{\sum_x \sum_y m(x,y)} \tag{4}$$

denotes averaging in two dimensions over all valid pixels $\mathbf{s}(x,y)$. A subscript is used to specify averaging in a certain dimension. For example

$$\langle s(p,x,y)\rangle_p = \frac{\sum_p m(x,y)s(p,x,y)}{P} \tag{5}$$

denotes averaging over all available channels.

2.5 Baseline

Many algorithms use the Along-Track Interferometry (ATI) baseline as a parameter. For multi-aperture modes (Moving Object Detection Experiment 2 (MODEX2)), there are different ways to define the baselines. The following channel enumeration (indexing order) is adopted for the two-way phase center separations $D(p)$ in the antenna frame of reference:

$$D(0) = 0 \tag{6}$$

$$D(p) > D(q) \text{ for } p > q \tag{7}$$

For the most used MODEX modes,

$$D(p) \approx pD, \tag{8}$$

corresponding to the model discussed in [1], except that in this report the distances are measured from the trailing (aft-most) phase center.

2.6 Steering Vectors

A steering vector $\mathbf{b}(\beta)$ is a vector function of the scalar variable β that takes the following form:

$$\mathbf{b}(\beta) = \begin{bmatrix} \exp(j4\pi\frac{D(0)}{\lambda}\beta) \\ \vdots \\ \exp(j4\pi\frac{D(p)}{\lambda}\beta) \\ \vdots \\ \exp(j4\pi\frac{D(P-1)}{\lambda}\beta) \end{bmatrix}. \tag{9}$$

3 Data Model in the Image Domain

All algorithms described in this document are applied in the image domain. However, the image may be formed using an offset in the DC, relative to the DC value that is appropriate for the clutter and stationary targets [2, 3].

This section briefly presents the underlying data model, which is necessary for a better understanding of the implemented algorithms, especially the algorithms for clutter suppression. Some, though not all, of the implemented algorithms presume the covariance model provided in this section.

3.1 Sample Model

Considering that all focusing algorithms create artifacts such as azimuth shift of moving targets and PRF ambiguities, the underlying model of the image samples includes several components:

$$s(p,x,y) = s_{\mathrm{m}}(p,x,y) + s_{\mathrm{c}}(p,x,y) + s_{\mathrm{a}}(p,x,y) + e(p,x,y) \tag{10}$$

Basically, at a given pixel position, the multi-channel signal sample is modeled as a superposition of the moving target signature $s_{\mathrm{m}}(p,x,y)$, clutter $s_{\mathrm{c}}(p,x,y)$ and additive noise $e(p,x,y)$, where moving target and clutter components originate from different geographical locations. Due to spectral aliasing, ambiguities of moving or stationary targets may appear in the image at the specific distances from the principal target signatures. In the model (10), the ambiguities from strong stationary (or moving) targets (often originating from a man-made construction) are represented by a separate component of the signal, $s_{\mathrm{a}}(p,x,y)$. Other ambiguities, which are always present to some extent, may be absorbed in the term $s_{\mathrm{c}}(p,x,y)$. For simplicity (and in practice), the number of signal components in (10) can be limited to two or three at any one particular pixel although in theory their number may be large [4]. The two components that are always assumed present are the system noise and clutter. They are present in all pixels. In some pixels there may be more significant contributors. For example, a third term may be a single moving target superimposed on the clutter and noise. At some image locations, a single strong ambiguity may be superimposed on the clutter and noise. It is possible that multiple overlaid moving targets get imaged at the same pixel location. It is also possible that a mix of targets and ambiguities occupy the same pixel. However, such cases are not very likely and will not be considered in further text.

Under idealized conditions, each term of (10) can be modeled as follows.

After focusing and coregistration, the moving target term can be expressed as:

$$\mathbf{s}_{\mathrm{m}}(x,y) = S_{\mathrm{m}}\mathbf{b}_{\mathrm{m}} = S_{\mathrm{m}}\mathbf{b}\left(\frac{V_{\mathrm{r}}}{V_{\mathrm{s}}}\right) \tag{11}$$

with unknown parameters: amplitude S_{m} and ATI phase. The latter is directly proportional to the ratio of the target's radial speed V_{r} and the antenna speed V_{s}. The amplitude may be considered unknown but deterministic or it may be considered random, presumably with a known distribution. Unless the mover is a point target, its amplitude S_{m} may vary across the surface of that same target. For a small distributed target, its ATI phase is assumed to be spatially constant. For a large

distributed target such as a ship, its ATI phase is assumed to be gradually variable over the image space that it occupies.

Similarly, the stationary clutter (the background target signature) may be modeled in the same way, with the ATI phase equal to zero:

$$\mathbf{s}_{\mathrm{c}}(x,y) = S_{\mathrm{c}}\mathbf{b}_{\mathrm{c}} = S_{\mathrm{c}}\mathbf{b}(0) \tag{12}$$

where the amplitude S_{c} is assumed unknown, either deterministic or random. The probability density function (pdf) associated with the stochastic clutter model is typically not Gaussian due to the image texture. Great simplifications in the detector derivation can be made if the clutter pdf can be considered as multivariate Gaussian.

Ambiguities $s_{\mathrm{a}}(p,x,y)$ can be modeled like moving or background targets in the form:

$$\mathbf{s}_{\mathrm{a}}(x,y) = S_{\mathrm{a}}\mathbf{b}_{\mathrm{a}} \tag{13}$$

where the specific phases in $\mathbf{b}_{\mathrm{a}}$ are similar to the mover ATI phases, but they depend on the system parameters and the applied DC offset (positive or negative). In particular, the ambiguity ATI phase of a stationary target is a combination of two terms [5]. The first is $\pm 2\pi D(p) f_{\mathrm{p}}/V_{\mathrm{s}}$, which depends on how close the system parameters are to the DPCA condition (which is $D = V_{\mathrm{s}}/f_{\mathrm{p}}$). The second part is either 0 or $\pm\pi$, introduced by transmitter or receiver time multiplexing for virtual multichannel modes (MODEX2 with $P = 4$). For a mover ambiguity, its ATI phase additionally depends on the mover radial speed. For the same target, S_{a} increases as more of target energy appears in the spectral alias (greater DC mismatch).

The above simplified model describes the various components as each belonging to a subspace of $\mathbb{C}^P$, spanned by $\mathbf{b}(\beta)$ or $\mathbf{b}_{\mathrm{a}}$.

The additive noise in the model (10) is a white Gaussian process with zero mean and variance σ_{e}^2. Noise components of different channels are statistically independent and identically distributed.

3.2 Covariance Matrix Model

If a stochastic target model is used, the target covariance matrix defines its second order statistics. It is assumed to be structured as follows:

$$\mathbf{C}_{\mathrm{m}} = \sigma_{\mathrm{m}}^2 \mathbf{b}_{\mathrm{m}} \mathbf{b}_{\mathrm{m}}^H \tag{14}$$

Detector derivation for stochastic targets is simplified if it can be assumed that the pdf of a stochastic target is multivariate Gaussian with zero mean and the structured covariance matrix as shown in (14). Then the pdf depends only on the unknown variance σ_{m}^2 and the unknown normalized radial speed (as a parameter in $\mathbf{b}_{\mathrm{m}}$).

Similarly, the clutter covariance matrix, used in the stochastic clutter model, may be structured as follows:

$$\mathbf{C}_{\mathrm{c}} = \sigma_{\mathrm{c}}^2 \mathbf{b}_{\mathrm{c}} \mathbf{b}_{\mathrm{c}}^H \tag{15}$$

Unlike (14), this expression has only one unknown, the clutter variance σ_c^2. This simplified structured model is exploited in some algorithms for clutter suppression. In other algorithms, no particular structure of $\mathbf{C}_c$ is presumed. In fact, the model (15) is not necessarily accurate because the clutter itself may contain a multitude of moving scattering facets (vegetation, ocean surface), mixed contributions from azimuth and range ambiguities, and the effects of uncalibrated channel imbalance. All these factors work to increase the rank of $\mathbf{C}_c$ from 1 up to possibly full rank.

In analogy with (14) and (15), one may write:

$$\mathbf{C}_a = \sigma_a^2 \mathbf{b}_a \mathbf{b}_a^H \tag{16}$$

when the ambiguity is believed to come from a random target and the only unknown parameter, σ_a^2, relates to the aliased energy. This value varies for a variable DC offset.

Since signal components in (10) are statistically independent, the covariance matrix $\mathbf{C}$ can be written as a sum of two or more component covariance matrices. Assuming all kinds of contributors, the covariance matrix is modeled as:

$$\mathbf{C} = \mathbf{C}_m + \mathbf{C}_c + \mathbf{C}_a + \sigma_e^2 \mathbf{I} \tag{17}$$

4 Sample Covariance and Coherence Matrices

Sample covariance and sample coherence matrices are used in the definition of many implemented algorithms. They are estimated from the data by massive averaging (in both dimensions taking into account masking), which makes the algorithms data-adaptive. The data are required to be in the image domain for all of the algorithms described in this report. Because of this, the sample covariance and coherence matrices are estimated in that domain.

4.1 Sample Covariance Matrix

The covariance matrix $\mathbf{C} \in \mathbb{C}^{P \times P}$ is estimated by averaging over all currently available data:

$$\mathbf{C} = \langle \mathbf{s}(x,y)\mathbf{s}(x,y)^H \rangle = \frac{\sum_{x,y} m(x,y)\mathbf{s}(x,y)\mathbf{s}(x,y)^H}{\sum_{x,y} m(x,y)} \tag{18}$$

This is the sample covariance matrix as opposed to the mathematical expectation of $\mathbf{s}(x,y)\mathbf{s}(x,y)^H$. In the definition of certain algorithms, the inverse, $\mathbf{C}^{-1}$, or the inverted square root, $\mathbf{C}^{-1/2}$, is needed. The latter is defined (and computed) as:

$$\mathbf{C}^{-1/2} = \sum_{k=1}^{P} \lambda_k^{-1/2} \mathbf{u}_k \mathbf{u}_k^H \tag{19}$$

where λ_k are the eigenvalues and $\mathbf{u}_k$ are the eigenvectors of $\mathbf{C}$.

4.2 Sample Coherence Matrix and Channel Balance

The coherence matrix $\mathbf{H} \in \mathbb{C}^{P \times P}$ is estimated by averaging over all currently available data and by normalizing the result:

$$[\mathbf{H}]_{p,q} = \frac{\langle s(p,x,y)s(q,x,y)^* \rangle_{x,y}}{\sqrt{\langle s(p,x,y)s(p,x,y)^* \rangle_{x,y}} \sqrt{\langle s(q,x,y)s(q,x,y)^* \rangle_{x,y}}} \tag{20}$$

As already mentioned, masking is implied in the averaging operation.

Coherence is computed as a complex scalar based on three averaged inner products. The same three averaged inner products, which form (20), are also used for simple (scalar) channel calibration. The phase of the numerator shows the bulk phase imbalance and is countered by the opposite calibration phase between channels p and q. The ratio of the two factors in the denominator provides the necessary level adjustment between these channels.

5 Projection Matrix for Clutter Cancellation

The projection matrix $\mathbf{P}^{\perp}$ is implemented as the projector to the orthogonal complement of the "clutter subspace" assuming that the clutter is spanned by the columns of a matrix $\mathbf{B}_{\mathrm{c}}$:

$$\mathbf{P}^{\perp} = \mathbf{I} - \mathbf{B}_{\mathrm{c}}(\mathbf{B}_{\mathrm{c}}^{H}\mathbf{B}_{\mathrm{c}})^{-1}\mathbf{B}_{\mathrm{c}}^{H} \tag{21}$$

The purpose of the projection matrix $\mathbf{P}^{\perp}$ is to cancel clutter or, at least, the main components of the clutter.

The clutter subspace can be defined in several ways (depending on the model), using a deterministic (geometry-based) method or an adaptive (balancing) method. Supported options, specified by user at run-time, are:

$$\mathbf{B}_{\mathrm{c}} = \begin{cases} [\ldots \mathbf{b}(\beta_k) \ldots] & \text{numerical} \\ \mathbf{b}(0) & \text{geometry, baseband} \\ \left[\mathbf{b}(0)\, \mathbf{b}_{\mathrm{spa}}\right] & \text{geometry, baseband and upper ambiguity} \\ \left[\mathbf{b}(0)\, \mathbf{b}_{\mathrm{spa}}^{*}\right] & \text{geometry, baseband and lower ambiguity} \\ \mathbf{b}_{\mathrm{bal}} & \text{balance} \end{cases} \tag{22}$$

where $\mathbf{b}(\cdot)$ is a steering vector as defined in (9) and $\mathbf{b}_{\mathrm{spa}}$ and $\mathbf{b}_{\mathrm{bal}}$ are special steering vectors defined below. It is noted here that $\mathbf{b}_{\mathrm{spa}}$ and $\mathbf{b}_{\mathrm{bal}}$ are closely related to the steering vectors $\mathbf{b}_{\mathrm{a}}$ and $\mathbf{b}_{\mathrm{c}}$, respectively, which introduced in section 3.2 for modeling the covariance matrix. The current version of the software does not support $\mathbf{B}_{\mathrm{c}}$ of rank larger than 2.

5.1 Clutter Subspace Defined Numerically

In the first option in (22), it is assumed that the clutter is spanned by steering vectors, $\mathbf{b}(\beta_k)$, where β_k for $0 \leq k < P$ are given numerically from an external source. These are the ATI values that will be notched out.

5.2 Basic DPCA Defined by Geometry

The next option is the simplest case, corresponding to the basic DPCA algorithm. In this case, it is assumed that all clutter samples are scaled versions of $\mathbf{b}(0)$. The justification for this choice is simple. Adopting the models (12) and (15), clutter samples are assumed to be identical in all coregistered channels. Then the projection matrix $\mathbf{P}^{\perp} = \mathbf{P}_0^{\perp}$ is given by:

$$\mathbf{P}_0^{\perp} = \mathbf{I} - \frac{1}{\mathbf{b}(0)^{H}\mathbf{b}(0)}\mathbf{b}(0)\mathbf{b}(0)^{H} \tag{23}$$

This type of projection should be applied to the data samples after channel balancing and spatial coregistration. In this case, $\mathbf{P}^{\perp}\mathbf{s}(x,y)$ removes the mean (computed over channels) $\langle s(p,x,y)\rangle_p = \mathbf{b}(0)^{H}\mathbf{s}(x,y)/P$ from each component of $\mathbf{s}(x,y)$. In other words, a notch is placed at ATI phase 0 and should notch out the baseband clutter. The argument of the steering vector is implicitly taken to be 0 based on geometry (all channels see the entire surface through the same geometry).

5.3 Clutter Components from Baseband and One Ambiguity Defined by Geometry

The next two options in (22) are modifications of the simple DPCA case, where it is again assumed that the samples have been balanced and spatially coregistered, but, possibly, processed with a DC offset, causing stronger clutter ambiguities. Using geometry calculations, it is easy to derive the phase mismatch of the clutter ambiguities, as a result of improper interpolation [5]. In fact,

$$\mathbf{b}_{\text{spa}} = \mathbf{b}_{\text{a}}^{*} \tag{24}$$

with reference to (13) and considering only ambiguities from stationary targets. The elements of $\mathbf{b}_{\text{a}}$, i.e. $\mathbf{b}_{\text{spa}}$ in (22) have been discussed in section 3.1. In some more detail, they are given by:

$$[\mathbf{b}_{\text{spa}}]_p = \exp(j2\pi f_{\text{p}} \zeta_{\text{spa}}(p)) = \exp(j2\pi \delta_{\text{spa}}(p)) \tag{25}$$

where $\zeta_{\text{spa}}(p)$ is the slow time shift necessary to achieve spatial coregistration between channel p and channel 0 and, in the equivalent formulation, $\delta_{\text{spa}}(p)$ is the normalized shift within the data grid (in terms of sample spacing $D_{\text{s}} = V_{\text{s}}/f_{\text{p}}$). As discussed in section 3.2, these normalized shifts are calculated by combining two parameters. The first one is the ratio between the phase center separation $D(p)$ and the slow time spacing D_{s}. The second one is the relative sampling delay between channels, in terms of Pulse Repetition Interval (PRI), in the time multiplex that is used for MODEX2, which is ± 0.5 or, in other words, $\pm 50\%$ of the PRI (the sign depends on the channel order on file). The values of the relative shifts $\delta_{\text{spa}}(p)$ are the same values as used for spatial coregistration if this operation is done explicitly (not adaptively). Besides the baseband, one of the ambiguities is selected for cancellation. Which ambiguity is selected for cancellation depends on the sign of the DC offset. If DC offset is positive (for capturing vehicles with negative radial speed), the upper ambiguity should be cancelled. For negative DC offset, the lower ambiguity should be cancelled. The implementation allows other options, such as notching both clutter ambiguities ($\mathbf{b}_{\text{spa}}$ and $\mathbf{b}_{\text{spa}}^{*}$), but not the baseband clutter. However, this option is not very useful.

5.4 Clutter Notch Positioned by Channel Balancing

The final option in (22) is based on the measured average (bulk) phase imbalance between channels, $\phi_{\text{bal}}(p) = \angle\langle s^{*}(p,x,y)s(0,x,y)\rangle$, as mentioned in section 4.2. This value is expected to be 0 after channel balancing. In other words,

$$\mathbf{b}_{\text{bal}} = \mathbf{b}_{\text{c}}^{*} \tag{26}$$

where $\mathbf{b}_{\text{c}}$, as estimated from the data, may slightly deviate from the deterministic vector $\mathbf{b}(0)$. Typically, the data-based $\mathbf{b}_{\text{c}}$ is close to the fixed $\mathbf{b}(0)$, but there may be some exceptions. In particular, some processing chains include focusing in combination with coregistration (interpolation) with a DC offset (suitable for movers) after original channel balancing. The DC offset then causes clutter ambiguities in the background image, with ambiguity ATI phases $\pm 2\pi\delta_{\text{spa}}(p)$, as already discussed. This disturbs the channel balance. When the DPCA condition is nearly met ($\delta_{\text{spa}}(p)$ close to an integer), it is possible that a single notch placed in between 0 ATI phase and $\pm 2\pi\delta_{\text{spa}}(p)$ may provide a good compromise between suppressing the baseband clutter and the ambiguous clutter. This option is based on measuring the phase imbalance between channels

$$\phi_{\text{bal}}(p) = \angle\langle s^{*}(p,x,y;f_{\text{c}})s(0,x,y;f_{\text{c}})\rangle \tag{27}$$

where it is symbolically indicated that processing (focusing with coregistration) has been carried out with a selected DC parameter f_c. The notch is placed adaptively to restore the channel balance:

$$[\mathbf{b}_{\text{bal}}]_p = \exp(j\phi_{\text{bal}}(p)) \tag{28}$$

6 Test Statistic for Quadrature Detector – Nonparametric Detection

This section describes a class of implemented quadrature detectors that are defined without any reference to the mover parameters. However, DC offset processing can be used even with this type of nonparamteric detection to increase the chance of capturing all of the mover energy [3] when forming the test statistic.

The input signal $\mathbf{s}(x,y)$ is assumed to be spatially coregistered. The test statistic $t(x,y)$ is evaluated for every pixel according to the following formula:

$$t(x,y) = 2\sum_{p=P_0}^{P-1} \frac{|\mathbf{b}_p^H \mathbf{s}_p(x,y)|^2}{\langle |\mathbf{b}_p^H \mathbf{s}_p(x,y)|^2 \rangle} \tag{29}$$

where weights $\mathbf{b}_p$, $p = P_0, \ldots, P$ can be defined in different ways. Averaging in the denominator of (29) goes over all valid samples and serves as a normalization factor.

A variation of this concept permits the use of different DC offset values for a different set of weights $\mathbf{b}_p$, so that data are refocused ($P - P_0$ times) prior to applying each of the weights and then the corresponding results are summed together. This option is explicitly indicated in the following modification of (29):

$$t(x,y) = 2\sum_{p=P_0}^{P-1} \frac{|\mathbf{b}_p^H \mathbf{s}_p(x,y; f_c(\mathbf{b}_p))|^2}{\langle |\mathbf{b}_p^H \mathbf{s}_p(x,y; f_c(\mathbf{b}_p))|^2 \rangle} \tag{30}$$

where the relation between f_c and $\mathbf{b}_p$ remains to be defined by the user (as the designer of the overall algorithm). While (29) is implemented in one of the *gmtipro2* modules, the modification (30) can be implemented (at run time) through an iteration of several modules.

6.1 Projection Based Quadrature Detector – DPCA

In the framework of the DPCA approach, orthogonal vectors $\mathbf{b}_p$ ($p = P_0, \ldots, P$) are chosen to span the "signal" subspace (the orthogonal complement of the P_0-dimensional clutter subspace) and $\mathbf{s}_p(x,y)$ in (29) stands for the image pixels focused with specific processing parameters (such as the processed Doppler bandwidth or spectral windows). There is a subtle difference between two implemented forms: $2\sigma_e^{-2}\mathbf{s}(x,y)^H \mathbf{P}_0^{\perp}\mathbf{s}(x,y)$ and (30). In the modified version (30), samples $\mathbf{s}_p(x,y; f_c(\mathbf{b}(p))$ are additionally assumed to be focused using a specific DC offset, which is adjusted to the weights $\mathbf{b}_p$. Partial detection results, corresponding to each $\mathbf{b}_p$ set, are also available.

For P=2, the only option is:

$$\mathbf{b}_1 = \mathbf{b}(\pi) = \frac{1}{\sqrt{2}} \begin{bmatrix} 1 \\ -1 \end{bmatrix} \tag{31}$$

since the background is assumed collinear with $\mathbf{b}_0 = \mathbf{b}(0)$.

For $P > 2$, there are various possibilities. An example of a suitable set of vectors $\mathbf{b}_p$ is defined by:

$$[\mathbf{b}_p]_q = \frac{1}{\sqrt{P}} \exp(j2\pi pq/P) \text{ for } q = 0, \ldots, P-1 \text{ and } p = 1, \ldots, P-1 \tag{32}$$

This is the set of Fourier vectors excluding $\mathbf{b}_0 = \mathbf{b}(0)$. Partial results from this variant of the DPCA detector are very close to the Velocity Synthetic Aperture Radar (VSAR) concept proposed in [6]. In the special case of $P = 4$, (32) becomes:

$$\left[\begin{array}{ccc} \mathbf{b}_1 & \mathbf{b}_2 & \mathbf{b}_3 \end{array} \right] = \frac{1}{2} \left[\begin{array}{ccc} 1 & 1 & 1 \\ j & -1 & -j \\ -1 & 1 & -1 \\ -j & -1 & j \end{array} \right] \tag{33}$$

and its partial outputs are tuned to three unambiguous radial speeds. Since $\mathbf{b}_p$ and $\mathbf{b}_{P-p}$ are approximately matched to radial speeds of the opposite signs (especially for a uniform linear array as in (8)), it makes sense to use opposite DC offsets for focusing $\mathbf{s}_p$ and $\mathbf{s}_{P-p}$. In other words, the applied DC offsets and the applied weights $\mathbf{b}_p$ within the same algorithm iteration should be simultaneously matched to either positive or negative radial speeds.

Another suitable option specifically for $P = 4$ is:

$$\left[\begin{array}{ccc} \mathbf{b}_1 & \mathbf{b}_2 & \mathbf{b}_3 \end{array} \right] = \frac{1}{2} \left[\begin{array}{ccc} 1 & 1 & 1 \\ 1 & -1 & -1 \\ -1 & -1 & 1 \\ -1 & 1 & -1 \end{array} \right] \tag{34}$$

These vectors are not directional (do not favor positive or negative radial speeds) and no meaningful selection of the DC offsets can be recommended. It is noted that $\mathbf{b}_1$ provides the largest gain for slow targets (of either sign) within this set.

6.2 Covariance Based Quadrature Detector – Full Rank Decorrelator

For this method, $P_0 = 0$ and

$$\left[\begin{array}{ccc} \mathbf{b}_0 & \cdots & \mathbf{b}_{P-1} \end{array} \right] = \mathbf{C}^{-1/2} \tag{35}$$

This special case of the test statistic can be represented in a different form. Considering that in this case

$$\mathbf{C}^{-1/2}\mathbf{s}(x,y) = \left[\begin{array}{c} \vdots \\ \mathbf{b}_p^H \mathbf{s}(x,y) \\ \vdots \end{array} \right] \tag{36}$$

and because

$$\langle \mathbf{C}^{-1/2}\mathbf{s}(x,y)\mathbf{s}(x,y)^H \mathbf{C}^{-1/2} \rangle = \mathbf{I} \tag{37}$$

it follows that diagonal elements of (37) satisfy

$$\langle \mathbf{b}_p^H \mathbf{s}(x,y)\mathbf{s}(x,y)^H \mathbf{b}_p \rangle = \langle |b_p^H \mathbf{s}(x,y)|^2 \rangle = 1 \tag{38}$$

and then, the test statistic (29) can be rewritten as:

$$t(x,y) = \mathbf{s}(x,y)^H \mathbf{C}^{-1} \mathbf{s}(x,y) \tag{39}$$

This form of the test statistic, which tends to decorrelate channels, is mathematically the same as that of a ship detector used on polarimetric imagery [7] (in which case it tends to decorrelate polarimetric channels).

The quadrature detector based on (35) (or (39)) has proven very useful for ocean applications. It may also be useful as a preliminary detector in a more complex algorithm. For example, it can be used to quickly detect and mask strong signatures of large ships, which leads to a more accurate measurement of the clutter statistics needed for further application of more advanced algorithms [8].

7 Test Statistic for Combined Detection and Estimation

The input signal $\mathbf{s}(x,y)$ is assumed to be spatially coregistered. The test statistic $t(x,y)$ is evaluated for every pixel according to the following set of formulae:

$$J(x,y,V_\mathrm{r};f_\mathrm{c}) = \frac{\sum_{d_x\in\mathbb{D}_x}\sum_{d_y\in\mathbb{D}_y}|\mathbf{b}(V_r/V_s)^H\mathbf{Q}(P-P_0;f_\mathrm{c})\mathbf{s}(x+d_x,y+d_y;f_\mathrm{c})|^2}{\mathbf{b}(V_r/V_s)^H\mathbf{Q}(P-P_0;f_\mathrm{c})\mathbf{b}(V_r/V_s)} \tag{40}$$

$$\hat{V}_\mathrm{r}(f_\mathrm{c}) = \arg\max_{V_\mathrm{r}\in\mathbb{D}_V} J(x,y,V_\mathrm{r};f_\mathrm{c}) \tag{41}$$

$$t(x,y) = \max_{f_\mathrm{c}\in\mathbb{D}_{f_\mathrm{c}}}\left(I(\hat{V}_\mathrm{r}(f_\mathrm{c})\in\mathbb{D}_{V_\mathrm{r}}(f_\mathrm{c}))J(x,y,\hat{V}_\mathrm{r};f_\mathrm{c})\right) \tag{42}$$

In accordance and in addition to the general notation introduced in Section 2, the following symbols are used:

$\mathbb{D}_{f_\mathrm{c}}$	The interval of test values for f_c
$\mathbf{s}(\cdot;f_\mathrm{c})$	Image pixel focused with a certain f_c value
V_r	Test radial speed of a moving target
$\mathbb{D}_V$	The interval of unambiguous values for V_r
$\mathbb{D}_{V_\mathrm{r}}(f_\mathrm{c})$	The interval of test values for V_r to be acceptable depending on the f_c parameter
d_x	Offset in the neighborhood of the current azimuth
$\mathbb{D}_x$	Support window in azimuth
d_y	Offset in the neighborhood of the current range
$\mathbb{D}_y$	Support window in range
$I(\cdot)$	Indicator function taking value 1 for true arguments and 0 for false arguments
$\mathbf{b}(\cdot)$	Test steering vector
$\mathbf{Q}(k;f_\mathrm{c})$	Kernel matrix of rank k, may vary with the applied f_c

The kernel $\mathbf{Q}(P-P_0;f_\mathrm{c})$, used to suppress the clutter in (40), is redefined for each of the specific methods of the same class. It may have full rank P or reduced rank $P-P_0$ where P_0 is the assumed rank of the clutter subspace. It may be estimated or constructed for each test value of f_c. It is emphasized here that the same kernel, which is used for clutter suppression, must also be used in normalization (the denominator of (40)).

In (40), summing the pixel contributions within a rectangular window, centered around (x,y), and defined by $\mathbb{D}_x$ and $\mathbb{D}_y$ is optional (set through design parameters at run-time). The default window is one sample wide, i.e. $\mathbb{D}_x=\{0\}$ and $\mathbb{D}_y=\{0\}$. This choice (and default setting) forces the algorithm to use a single pixel value $\mathbf{s}(x,y;f_\mathrm{c})$ when evaluating the criterion $J(x,y,V_\mathrm{r};f_\mathrm{c})$, which is then used to estimate the radial speed in (41) and to compute the test statistic $t(x,y)$ in (42).

Focusing may be done with a variable DC offset, while the other focusing parameters (Doppler rate, processed bandwidth and spectral window shape) are kept constant according to the general algorithm formulation (40), (41), (42). Normally, these fixed parameters take the appropriate or default values, but they too may be modified by the user as design parameter at run time. Multiple DC offset values can be used iteratively in order to evaluate $t(x,y)$ defined in (42). The set of suitable

test DC offsets is provided to the algorithm externally (as a design parameter) either directly as frequency offsets from the dominant (bulk clutter) DC or as a set of preliminary test V_{r} values. These preliminary test values are supposed to be given in coarse steps. For each DC offset (or preliminary test V_{r}), a large, denser, set of V_{r} values is tested on a finer scale (in finer steps) using (41). The fine-scale estimates from (41) are then checked against the expected domain $\mathbb{D}_{V_{\mathrm{r}}}(f_{\mathrm{c}})$ to see if they are actually matching the coarse-level setting used in focusing. If this is the case, the estimate produced by (41) is accepted, otherwise it is rejected. In the latter case, it is very likely that the non-matching estimate originates from a mover ambiguity. By this method, the detection candidates are censored. Partial maximization results (uncensored) from (41) for each fixed f_{c} are also available as algorithm output.

The test statistic $t(x,y)$ of (42) is used for moving target detection by comparison to a suitable threshold. The value $\hat{V}_{\mathrm{r}}$ that achieves the maximum globally over all f_{c} is an estimate of the target's radial speed.

7.1 Reduced Rank Kernel – DPCA with Adaptive Steering

One option for choosing the kernel matrix is to notch out the clutter using any one form of the projection matrix (based on numerical input, geometry calculations or balance measurements) as discussed in Section 5 and then to normalize it by an estimate of the residual power $\hat{\sigma}_e^2$, which may change with f_{c}.

$$\mathbf{Q}(P-P_0) = 2\hat{\sigma}_{\mathrm{e}}^{-2}\mathbf{P}^{\perp} \tag{43}$$

The reduced rank of the kernel, $P-P_0 < P$, is as discussed in section 6.1. Additionally, the projection matrix may change with f_{c} if it is derived from the balance results, $\phi_{\mathrm{bal}}(p)$. If the projection matrix is based only on the geometry considerations, then it may depend on the sign of the DC offset (the difference between f_{c} used in focusing and the DC value corresponding to the bulk ground backscatter), as noted in Section 5.

This type of detector is described in detail in [9]. In broad terms, it is closely related to the Notch Periodogram (NP) concept [10, 11].

7.2 Full Rank Kernel – Adaptive Matched Steering

The option given by

$$\mathbf{Q}(P) = \mathbf{C}^{-1} \tag{44}$$

is to decorrelate or whiten the channels using the sample covariance matrix as discussed in Section 4.1. With this option, $\mathbf{C}$ defined in Section 4.1 actually changes with f_{c} due to a change in the ratio of the ambiguity to baseband power.

This type of test statistic is discussed in numerous papers (e.g. [12]).

8 Detection Thresholds

Detection is declared when the test statistic $t(x,y)$ surpasses the detection threshold η. With the current implementation, the threshold can be set directly or indirectly.

All test statistics presented in sections 6 and 7 are normalized to make the choice of the threshold easier. If η is set externally, directly as a number, it may loosely be interpreted as the relative level above the power of the residuals after clutter suppression.

A higher threshold, used on the same test statistic, decreases the Probability of False Alarms (PFA), but it also decreases the Probability of Detection (PD). The relationship between η and PFA (or PD) for a given form of test statistic depends on the pdf of the measurements and, in general, is very difficult to derive analytically. By setting the allowed PFA, the choice of η is indirectly made through certain implemented expressions that are not necessarily accurate. The implemented expressions are set for special cases and under special conditions. When applied to other cases, they produce a value for η which does not necessarily guarantee the preselected PFA.

The details regarding the threshold depend on the type of the test statistic and differ between the non-parametric and parametric detectors, projection-based and full-rank clutter suppression, single-pixel and multi-pixel test statistics. The common assumption for all is the assumption of Gaussian pdf of the single pixel complex residuals.

8.1 Detection Threshold for Nonparametric CFAR Detectors

The detection threshold η is determined to satisfy the equation:

$$1 - P_{\text{fa}} = \int_0^{\eta} p_0(z;\nu)dz \tag{45}$$

where P_{fa} is the chosen probability of false alarms, $\nu = 2n$ is the known or estimated value of the Degrees of Freedom (DOF) and $p_0(z)$ is the assumed pdf of the statistic z under the hypothesis that no moving target is present. In the current implementation, it is assumed that this pdf is χ^2, which has the following form

$$p_0(z;\nu) = \frac{z^{n-1}e^{-z/2}}{2^n\Gamma(n)} \tag{46}$$

where $\Gamma(\cdot)$ is the gamma function and the DOF depends on the method used in computing the statistic z. For example, if the projection-based quadrature detector of section 6.1 is used, then $z = t(x,y)$ has $2(P-P_0)$ DOF (where, typically $P_0 = 1$, or maybe $P_0 = 2$). For this detector, the test statistic is designed to cancel clutter leaving only the Gaussian thermal noise. Under such assumptions of Gaussian samples (in the absence of targets), the test statistic has indeed the χ^2 pdf. If the full rank non-parametric detector of section 6.2 is used, the same approach is valid (with $P_0 = 0$) if the additional assumption is made, namely that the residual clutter is Gaussian.

In these cases, the DOF can be set directly or estimated from the data, as stated in section 8.3.

8.2 Detection Threshold for Parametric CFAR Detectors with Adaptive Steering

In the case of the detector described in Section 7, taking $z = J(x, y, V_r; f_c)$ one would expect the DOF to be 2 (for no spatial averaging), or to be related to the estimated Equivalent Number of Looks (ENL) according to Section 8.3 (after spatial averaging). The χ^2 property would be justified either assuming full clutter suppression via projection or assuming that the residual clutter is Gaussian. Either way, the relationship between η and P_{fa}, given by (45) and (46) is good only for the partial criterion (40). The relationship is good for any, arbitrary value of V_r in (40), but it is not valid for the final test statistic (42).

Nonetheless, if the threshold is given indirectly, it is computed as in section 8.1 and it provides the prescribed P_{fa} per test case, but the overall PFA, P_{FA} is actually higher.

8.3 Equivalent Number of Looks

The implemented method for estimating the ENL, n, and DOF, $\nu = 2n$, is:

$$\nu = 2n = 2\frac{\langle S(p,x,y)\rangle^2}{\langle S^2(p,x,y)\rangle} \tag{47}$$

$$S(p,x,y) = |s(p,x,y)|^2 \tag{48}$$

where averaging and masking are applied as explained in Section 2.

9 Doppler Estimation and Analysis

The DC offset, which is used in some detectors, is applied relative to the DC of the background clutter. This section described the DC estimator that is implemented to estimate the bulk clutter DC.

The DC estimator uses the phase increment method to compute the localized DC, estimated independently at different fast time intervals. Then, an over-all DC model is fitted to the local estimates.

9.1 Local DC Estimation

The average phase increment is based on the autocovariance:

$$\overline{C(\tau)} = \sum_{\zeta} m(\zeta,\tau)m(\zeta+\Delta\zeta,\tau)s^*(\zeta,\tau)s(\zeta+\Delta\zeta,\tau), \tag{49}$$

which is also called the Average Cross Correlation Coefficient (ACCC) [13]. Here, $\Delta\zeta$ is the PRI. The angle (or phase) of the ACCC is given by

$$\phi_{\text{accc}}(\tau) = \angle\left(\overline{C(\tau)}\right). \tag{50}$$

The "raw" baseband DC estimate is then computed by

$$\hat{f}_{\text{c}}(\tau) = \frac{f_{\text{p}}}{2\pi}\phi_{\text{accc}}(\tau) \tag{51}$$

9.2 Smooth DC Estimates

A suitably biased version of this estimate is expressed as:

$$\hat{f}_{\text{b}}(\tau) = \frac{f_{\text{p}}}{2\pi}\angle\left(e^{j\phi_{\text{accc}}(\tau)}e^{-j\theta}\right) \tag{52}$$

$$\cos(\theta) = \frac{\langle\cos(\phi_{\text{accc}}(\tau)\rangle_{\zeta}}{\sqrt{\langle\cos(\phi_{\text{accc}}(\tau))\rangle_{\zeta}^2 + \langle\sin(\phi_{\text{accc}}(\tau))\rangle_{\zeta}^2}} \tag{53}$$

$$\sin(\theta) = \frac{\langle\sin(\phi_{\text{accc}}(\tau)\rangle_{\zeta}}{\sqrt{\langle\cos(\phi_{\text{accc}}(\tau))\rangle_{\zeta}^2 + \langle\sin(\phi_{\text{accc}}(\tau))\rangle_{\zeta}^2}} \tag{54}$$

where averaging goes over all processed slow time ζ and implies masking, as described in Section 2. The introduced bias is towards 0 and away from $\pm f_{\text{p}}/2$, which serves to avoid ambiguities in further processing [14]. Linear fitting with respect to fast time τ and removal of outliers are performed on the biased sequence $\hat{f}_{\text{b}}(\tau)$ defined by (52), not on the original unbiased sequence $\hat{f}_{\text{c}}(\tau)$ of (51). The domain of valid samples $\mathbb{D}_{\tau}$ is defined as:

$$\mathbb{D}_{\tau} = \left\{\tau|(\hat{f}_{\text{b}}(\tau) - f_{\text{lin}}(\tau))^2 < \alpha\langle(\hat{f}_{\text{b}}(\tau) - f_{\text{lin}}(\tau))^2\rangle_{\tau}\right\} \tag{55}$$

where $f_{\text{lin}}(\tau)$ is the linear fit to the biased estimates $\hat{f}_{\text{b}}(\tau)$ as defined by (52) and α is a given constant. The sequence of outlier-free DC estimates, $\tilde{f}_{\mathbf{c}}(\tau)$, is then obtained as:

$$\tilde{f}_{\mathbf{c}}(\tau) = \hat{f}_{\text{b}}(\tau) + \frac{f_{\text{p}}}{2\pi}\theta\,, \;\; \tau \in \mathbb{D}_{\tau} \tag{56}$$

and the final fit is performed on $\tilde{f}_{\mathbf{c}}(\tau)$ over the domain $\mathbb{D}_{\tau}$ to compute the coefficients of the Doppler polynomial.

For the computation of the DC map, as part of DC analysis, averaging is applied in both directions within small moving windows:

$$\hat{f}_{\text{c}}(\tau,\zeta) = \angle\langle\langle s(\zeta,\tau)\rangle^{*}_{\tau_c}\langle s(\zeta+\Delta\zeta,\tau)\rangle_{\tau_c}\rangle_{\zeta_c}, \tag{57}$$

where $\hat{f}(\tau,\zeta)$ is the Doppler centroid estimate calculated from the $\tau_c \times \zeta_c$ data chip centered at (τ,ζ).

10 Conclusion

Detectors described in this report represent one class of detectors that are implemented in *gmtipro2*. They have many commonalities. They all include a mechanism of suppressing the clutter based on known global properties of the clutter, which are given *a priori* or previously estimated on the entire data set.

Within this class, the described detectors can be divided into two groups:

– DPCA detectors are based on matrix projection; they make use of the assumption that the clutter lies in the clutter subspace of a low rank (1 or 2), which is, as a rule, *a priori* known.

– Full rank detectors make use of the noisy clutter covariance matrix, which needs to be estimated from the data using global averaging.

Another classification is also applicable to the described detectors:

– Nonparametric detectors are based on a test statistic in the quadratic form without any reference to any signal parameters.

– Parametric detectors imply certain target parameters; since true target parameters are *a priori* unknown, these detectors typically perform multiple tests and maximization over the parameter space.

Yet another view can be added to this type of detectors:

– Single-sample detectors work on a single image sample to generate the test statistic, which is then compared to a threshold.

– Multiple-sample detectors can use several neighboring samples to compute the test statistic; they work on sliding windows and their thresholds must be adjusted accordingly.

All of the detectors, by their design, can benefit from iterative processing with different DC offsets.

The described class of algorithms offers a great degree of flexibility at run time. To exploit the full potential of the implemented *gmtipro2* modules and plug-ins, the user must become familiar with their functional formulation, but not necessarily with their implementation aspects.

Evaluation of the algorithm performance is beyond the scope of this document. Two examples are shown in the Annex for illustration purposes only. The first example illustrates the algorithm effectiveness for land applications, and the second demonstrates the algorithm application in a maritime scene. Both examples show the results of combined detection and estimation of moving vehicles as delivered by the *gmtipro2* processor. The estimated target locations are shown overlaid on the background image, color coded according to their estimated radial speeds.

References

[1] Chiu, S. (2010), Moving target parameter estimation for RADARSAT-2 Moving Object Detection EXperiment (MODEX), *International Journal of Remote Sens.*, 31(15), 4007–4032.

[2] Dragošević, M. V. and Chiu, S. (2009), Space-Based Motion Estimators - Evaluation With the First RADARSAT-2 MODEX Data, *IEEE Geosci. and Remote Sens. Letters*, 6(3), 438–442.

[3] Chiu, S. and Dragošević, M. (2011), An efficient algorithm for fully capturing a ground moving target's energy for spaceborne SAR-GMTI, In *Proc. of RadarCon'11*, Kansas City, Kansas.

[4] Livingstone, C. and Dragošević, M. (2011), SAR-GMTI phasor sums and their impact on target velocity measurements, (DRDC TR 2011-177) Defence Research and Development Canada – Ottawa.

[5] Chiu, S. and Dragošević, M. (2010), Moving target indication via RADARSAT-2 multichannel synthetic aperture radar processing, *EURASIP Journal on Advances in Signal Processing*, Vol. 2010.

[6] Friedlander, B. and Porat, B. (1997), VSAR: a high resolution radar system for detection of moving targets, *Radar, Sonar and Navigation, IEE Proceedings*, 144(4), 205–218.

[7] Liu, C., Wachon, P., and Geling, G. (2005), Improved Ship Detection with Airborne Polarimetric SAR Data, *Can. J. Remote Sensing*, 31(1), 122–131.

[8] Dragosevic, M., Chiu, S., and Burwash, W. (2012), On ship sigantures in multi-aperture SAR images, In *Proc. IET Radar 2012*, Glasgow, UK.

[9] Dragosevic, M., Burwash, W., and Chiu, S. (2012), Detection and Estimation with RADARSAT-2 Moving Object Detection Experiment Modes, *IEEE TGRS*, 50(9), 3527–3543.

[10] Hwang, J. K. and Chen, Y.-C. (1993), Superresolution frequency estimation by alternating notch periodogram, *IEEE Transactions on Signal Processing*, 41(2), 727 –741.

[11] Macleod, M. (2001), Joint detection and high resolution ML estimation of multiple sinusoids in noise, In *Proceedings. (ICASSP '01). 2001 IEEE International Conference on Acoustics, Speech, and Signal Processing*, Vol. 5, pp. 3065 –3068.

[12] Budillon, A., Evangelista, A., and Schirinzi, G. (2012), GLRT Detection of Moving Targets via Multibaseline Along-Track Interferometric SAR Systems, *IEEE Geosci. and Remote Sens. Letters*, 9(3), 348 –352.

[13] Cumming, I. and Wong, F. (2005), Digital processing of synthetic aperture radar data: algorithms and implementation, Ch. 12, Norwood, MA: Artech House.

[14] Dragošević, M. (2009), Parametric Methods for Strip-Map SAR Doppler Ambiguity Resolution, *IEEE Trans. Aerospace and Electronic Systems*, 45(3), 869 –884.

Annex A: Algorithm Output Examples

Two processing examples are shown to illustrate the output of the presented combined detection and estimation algorithm. Both outputs were generated using the *gmtipro2* processor on selected RADARSAT-2 data.

Fig. A.1 is a composite image of the Ottawa region. The background is an optical image from a commercial source, which also includes the roadmap. The overlaid detections/estimations of moving vehicles come from *gmtipro2*. The detection/estimation results are accumulated from multiple RADARSAT-2 ascending and descending passes in MODEX1 and MODEX2 modes. Detected vehicles are presented by color-coded points where color represents their estimated speed. Traffic patterns can be observed in a qualitative way. This is a reprint of the poster prepared for the EUSAR 2012 best image contest.

Fig. A.2 is a SAR image of the Gibraltar region with overlaid ship detections/estimations. Both the SAR image and the ship results were produced by *gmtipro2* from an evening RADARSAT-2 pass in MODEX1 mode. Most ships are visible in the SAR image. They are shifted in azimuth from their estimated positions. Detected vessels are presented by color-coded points where color represents their estimated speed. The observed azimuth shifts correspond to these estimated speeds in sign and magnitude. Littoral and ship ambiguities are also visible in the SAR image. They are resolved automatically by *gmtipro2* after detection. This is a reprint of the result prepared for the Radar conference [8].

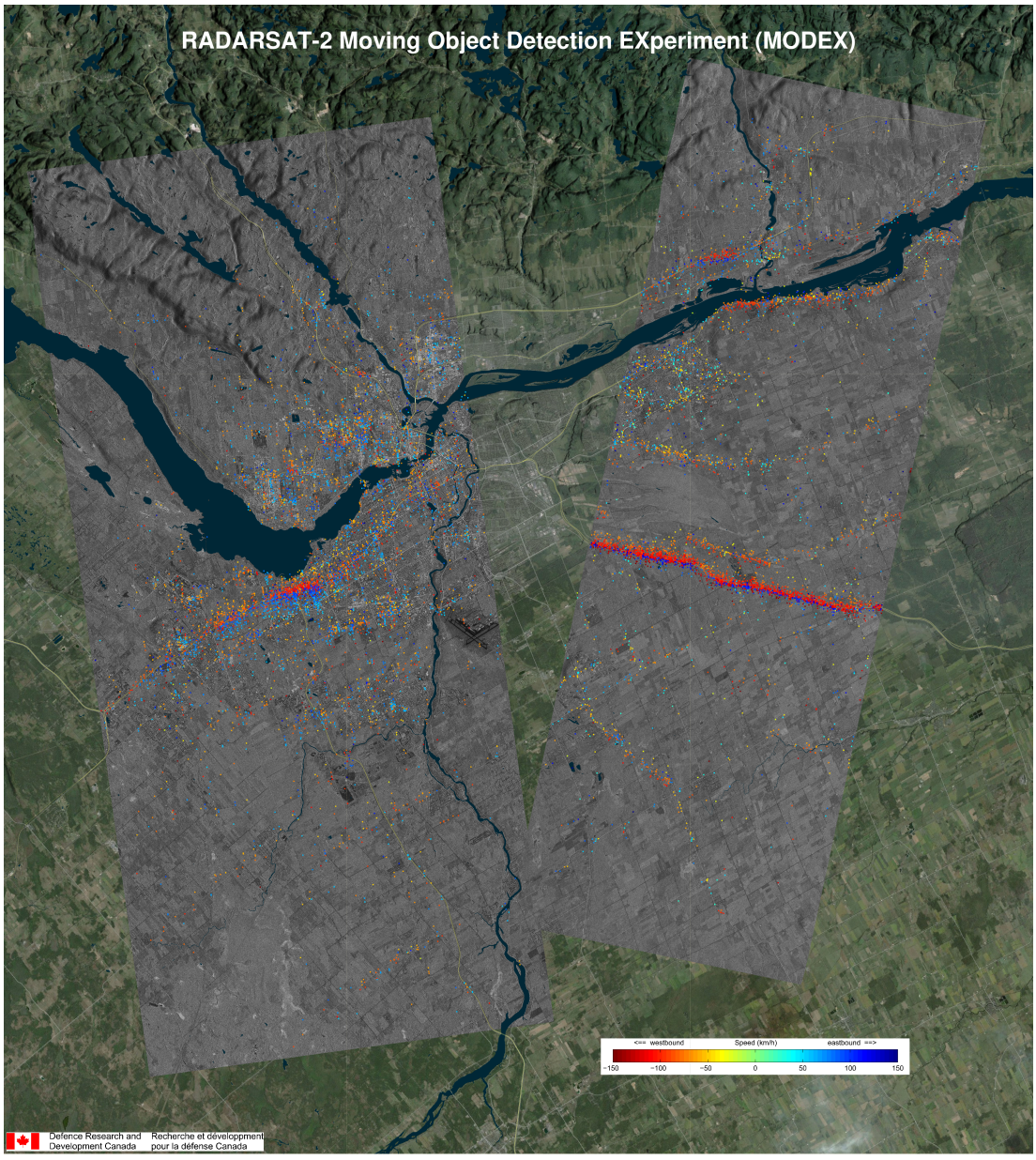

Figure A.1: *A composite image of the Ottawa region with overlaid detections/estimations of moving vehicles.*

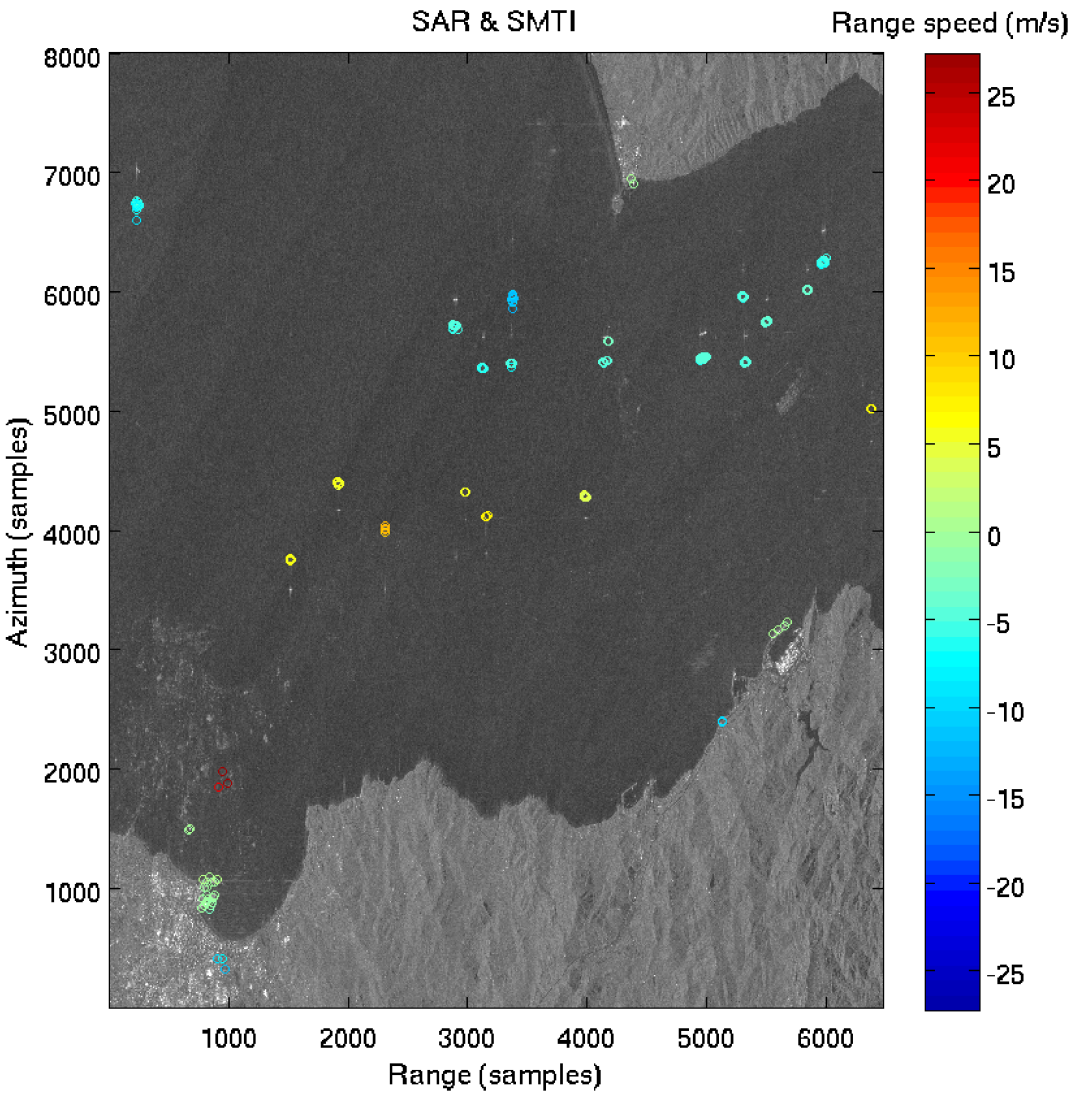

Figure A.2: *SAR image of the Gibraltar region with overlaid ship detections/estimations.*

This page intentionally left blank.

List of acronyms

ACCC Average Cross Correlation Coefficient

ATI Along-Track Interferometry

CFAR Constant False Alarm Rate

DC Doppler Centroid

DOF Degrees of Freedom

DPCA Displaced Phase Centre Antenna

DRDC Defence Research and Development Canada

ECEF Earth-Centered, Earth-Fixed

ENL Equivalent Number of Looks

GLRT Generalized Likelihood Ratio Test

LRT Likelihood Ratio Test

ML Maximum Likelihood

MODEX Moving Object Detection Experiment

MODEX1 Moving Object Detection Experiment 1

MODEX2 Moving Object Detection Experiment 2

NP Notch Periodogram

PD Probability of Detection

pdf probability density function

PFA Probability of False Alarms

PRF Pulse Repetition Frequency

PRI Pulse Repetition Interval

SAR Synthetic Aperture Radar

SMTI Surface Moving Target Indicator

VSAR Velocity Synthetic Aperture Radar

XML eXtensible Markup Language

This page intentionally left blank.

DOCUMENT CONTROL DATA

(Security markings for the title, abstract and indexing annotation must be entered when the document is Classified or Designated.)

1. ORIGINATOR (The name and address of the organization preparing the document. Organizations for whom the document was prepared, e.g. Centre sponsoring a contractor's report, or tasking agency, are entered in section 8.)

MDA Systems Ltd.
75 Albert Street, Suite 412
Ottawa, ON K1P 5E7

2a. SECURITY MARKING (Overall security marking of the document, including supplemental markings if applicable.)

UNCLASSIFIED

2b. CONTROLLED GOODS

(NON-CONTROLLED GOODS)
DMC A
REVIEW: GCEC APRIL 2011

3. TITLE (The complete document title as indicated on the title page. Its classification should be indicated by the appropriate abbreviation (S, C or U) in parentheses after the title.)

A Class of CFAR Detectors Implemented in the SAR-GMTI Processor *gmtipro2* : Mathematical Formulation of the Algorithms

4. AUTHORS (Last name, followed by initials – ranks, titles, etc. not to be used.)

Dragošević, M.; Burwash, W.

5. DATE OF PUBLICATION (Month and year of publication of document.)	6a. NO. OF PAGES (Total containing information. Include Annexes, Appendices, etc.)	6b. NO. OF REFS (Total cited in document.)
February 2015	40	14

7. DESCRIPTIVE NOTES (The category of the document, e.g. technical report, technical note or memorandum. If appropriate, enter the type of report, e.g. interim, progress, summary, annual or final. Give the inclusive dates when a specific reporting period is covered.)

Contract Report

8. SPONSORING ACTIVITY (The name of the department project office or laboratory sponsoring the research and development – include address.)

Defence Research and Development Canada – Ottawa
3701 Carling Avenue, Ottawa ON K1A 0Z4, Canada

9a. PROJECT OR GRANT NO. (If appropriate, the applicable research and development project or grant number under which the document was written. Please specify whether project or grant.)	9b. CONTRACT NO. (If appropriate, the applicable number under which the document was written.)
05eq	W7714-081104/001/SV

10a. ORIGINATOR'S DOCUMENT NUMBER (The official document number by which the document is identified by the originating activity. This number must be unique to this document.)	10b. OTHER DOCUMENT NO(s). (Any other numbers which may be assigned this document either by the originator or by the sponsor.)
DRDC Ottawa CR 2013-089	

11. DOCUMENT AVAILABILITY (Any limitations on further dissemination of the document, other than those imposed by security classification.)

(X) Unlimited distribution
( ) Defence departments and defence contractors; further distribution only as approved
( ) Defence departments and Canadian defence contractors; further distribution only as approved
( ) Government departments and agencies; further distribution only as approved
( ) Defence departments; further distribution only as approved
( ) Other (please specify):

12. DOCUMENT ANNOUNCEMENT (Any limitation to the bibliographic announcement of this document. This will normally correspond to the Document Availability (11). However, where further distribution (beyond the audience specified in (11)) is possible, a wider announcement audience may be selected.)

Unlimited

13. ABSTRACT (A brief and factual summary of the document. It may also appear elsewhere in the body of the document itself. It is highly desirable that the abstract of classified documents be unclassified. Each paragraph of the abstract shall begin with an indication of the security classification of the information in the paragraph (unless the document itself is unclassified) represented as (S), (C), or (U). It is not necessary to include here abstracts in both official languages unless the text is bilingual.)

This document provides a detailed mathematical description of several detection algorithms that have been implemented in the SMTI processor *gmtipro2* and tested on the actual SAR data from RADARSAT-2 acquired in the MODEX mode. The common feature of the described algorithms is their CFAR property. All of the detectors are generalized with respect to the number of available channels. Thus, they are defined both for MODEX1 and MODEX2 modes, which have two physical and four virtual channels, respectively. All of the detectors work in the image domain, but can be combined with DC offset focusing in order to integrate all signal energy and to improve the probability of detection. DC estimation, as one of the most important auxiliary algorithms, is also presented in the form of mathematical equations. The emphasis of the report is entirely on the mathematical formalism behind the computer code that implements these algorithms. Open literature references are provided regarding the derivation and analysis of these algorithms.

14. KEYWORDS, DESCRIPTORS or IDENTIFIERS (Technically meaningful terms or short phrases that characterize a document and could be helpful in cataloguing the document. They should be selected so that no security classification is required. Identifiers, such as equipment model designation, trade name, military project code name, geographic location may also be included. If possible keywords should be selected from a published thesaurus. e.g. Thesaurus of Engineering and Scientific Terms (TEST) and that thesaurus identified. If it is not possible to select indexing terms which are Unclassified, the classification of each should be indicated as with the title.)

Ground Moving Target Indication
Synthetic Aperture Radar
SAR
C-Band Spaceborne
Detection
Estimation
Constant False Alarm
CFAR
Test Statistic
Generalized Likelihood Ratio Test
GLRT
Maximu Likelihood
ML
Signal Processing